ROYAL SOCIETY OF CHEMISTRY

COMMUNICATION

Check for updates

Mechanical milling processed highly luminescent Cs–Pb–Br perovskite emitters†

Teng Zhang, [iD] *[a] Youru Bai,[a] Shaohuan Feng,[a] Qifan Xue, [iD] *[bc] Xiaotian Hu, [iD] *[d] Xueqing Xu,*[c] Heyuan Liu, [iD] [a] Yuriy N. Luponosov, [iD] [e] Muhammad Bilal Khan Niazi[f] and Xiyou Li [iD] *[a]

We report well-dispersed highly emitting perovskite emitters synthesized *via* the surfactant-assisted ball-milling method. Both the emitting peaks and the colour purity of the synthesized perovskite emitters can be effectively tuned through additive functionalization and precursor engineering.

In the past decade, lead halide perovskites with the ABX₃ structure have shown great potential in many optoelectronic fields including solar cells,[1–3] light-emitting diodes[4–7] and photodetectors.[8,9] In terms of light-emitting and displays, all inorganic CsPbX₃ (X = Cl, Br, I) nanocrystals (NCs) are most attractive due to their low exciton binding energy and colour tuning features.[10] To be more specific, different research groups have reported the successful synthesis of CsPbX₃ (X = Cl, Br, I) NCs with a near-unity photoluminescence quantum yield (PLQY).[11,12] The full width at half maxima (FWHM) of the emission spectra were less than 20 nm,[13,14] thus guaranteeing the colour purity of the synthesized emitters. The emission peak of the synthesized CsPbX₃ (X = Cl, Br, I) NCs can be tuned from 410–700 nm *via* compositional engineering, covering the whole visible light spectrum.[11]

Hot injection (HI),[15–17] ligand-assisted precipitation (LARP)[18–20] and mechanical milling[21,22] are widely used to prepare high-quality perovskite NCs. Different from the HI and LARP methods, mechanical milling avoided the massive use of organic solvents. Besides, the strong repeatability and energy-saving features make mechanical milling promising for industrialization. S. Eslava reported the gram-scale synthesis of CsPbBr₃ NCs through mechanical milling.[23] M. V. Kovalenko suggested that the solvents and capping ligands were essential during the preparation of highly emissive mechanical milling processed perovskite NCs.[24] H. Zhang introduced the facial synthesis of compositional engineered cesium lead halide perovskite NCs.[22]

The phase complexity of the synthesized Cs–Pb–Br component was also a problem. To be more specific, CsPbBr₃ with an emission wavelength near 510 nm has been widely investigated for light-emitting applications.[22–24] However, the synthesized Cs–Pb–Br emitters are frequently composed of a mixture of zero-dimensional (0D) Cs₄PbBr₆, two-dimensional (2D) CsPb₂Br₅ and three-dimensional (3D) CsPbBr₃. It has been reported that the three phases can be transformed reversibly with the assistance of solvent and ligand.[25–27] Besides, the emitting characteristics of the synthesized Cs–Pb–Br compound were structure and composition sensitive.[28] Instead of green emitting, J. Tian reported the blue emission of core–shell structured CsPbBr₃@amorphous CsPbBrₓ.[17] Blue emission has also been observed in CsPb₂Br₅ nanocrystals.[29] It has been reported that a CsPbBr₃@Cs₄PbBr₆ core–shell structure can reduce the aggregation tendency of the emitting CsPbBr₃ NCs.[28,30] A similar situation can be expected for the CsPbBr₃–CsPb₂Br₅ nanostructures.[31,32] Very recently, *via* precursor engineering, T. Lee reported ball-milled CsPbBr₃-decorated Cs₄PbBr₆ heterostructures for light emitting applications.[33] Compared with the HI and LARP methods, it seems that mechanical milling is advantageous in the controlled synthesis of highly luminescent structure-varied Cs–Pb–Br emitters.

In this study, the ball milling method has been selected to synthesize Cs–Pb–Br perovskite emitters. To start with, the

a School of Materials Science and Engineering, China University of Petroleum (East China), Qingdao, 266580, P. R. China. E-mail: tzhangae@connect.ust.hk, xiyouli@upc.edu.cn

b State Key Laboratory of Luminescent Materials and Devices, Institute of Polymer Optoelectronic Materials and Devices, School of Materials Science and Engineering, South China University of Technology, Guangzhou 510640, P. R. China
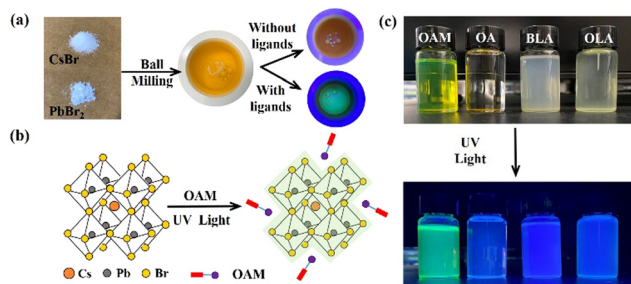
c Key Laboratory of New and Renewable Energy Research and Development, Guangzhou Institute of Energy Conversion, Chinese Academy of Sciences, Guangzhou 510640, P. R. China

d College of Chemistry and Chemical Engineering/Institute of Polymers and Energy Chemistry (IPEC)/Jiangxi Provincial Key Laboratory of New Energy Chemistry, Nanchang University, 999 Xuefu Avenue, Nanchang 330031, China

e Enikolopov Institute of Synthetic Polymeric Materials of the Russian Academy of Sciences, Moscow 117393, Russia

f School of Chemical & Materials Engineering, National University of Sciences & Technology, Islamabad, Pakistan

† Electronic supplementary information (ESI) available: Experimental details, Milling ball dependent PL characteristics (Fig. S1), FTIR spectrum of surfactant functionalized Cs–Pb–Br NCs (Fig. S2), TEM characterizations (Fig. S3) and stability evaluation (Fig. S4). See DOI: https://doi.org/10.1039/d3cc01345f

Fig. 1 (a) Photographs of the ball-milling processed Cs−Pb−Br perovskite emitter used in this study. (b) The schematic illustration of the light-emitting mechanisms for the OAM-functionalized perovskite emitters. (c) Photographs of the ambient light illuminated (upper c) and UV light illuminated (bottom c) different surfactant functionalized Cs−Pb−Br emitters dispersed in toluene.

influence of different surfactants has been investigated in detail. The oleic acid (OA) functionalized Cs−Pb−Br powders were not emissive, while the octylamine (OLA), butyl amine (BLA) and oleylamine (OAM) passivation resulted in blue, green and cyan emission. Detailed investigations showed that the OAM functionalized Cs−Pb−Br NCs exhibited the highest PLQY among the three long-chain amine surfactants. Shown in the steady-state photoluminescence (PL) spectrum, two distant peaks at 453 nm and 515 nm can be observed in the OAM passivated Cs−Pb−Br emitters, mainly due to the coexistence of $CsPbBr_3$ and $CsPb_2Br_5$. Finally, *via* precursor engineering, monochromatic green emitting NCs (PLQY 86.11%) with sharp emission characteristics (full width at half maximum (FWHM) of 21 nm) were synthesized. This research opened a new avenue for the facial and large-scale synthesis of high-quality colour-tuning perovskite emitters.
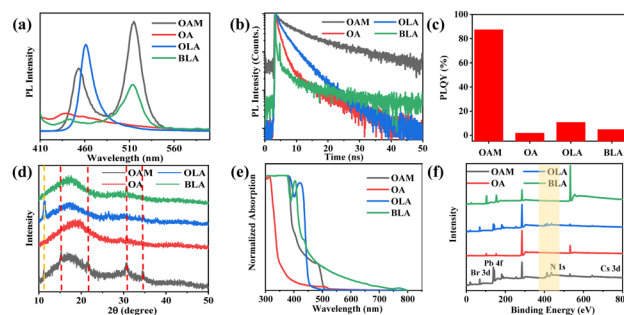
Fig. 1a shows the detailed description of the ball-milling processed Cs−Pb−Br emitters. $PbBr_2$ and CsBr have been mixed in the milling cans and the milling time has been set to 0.5 h. To start with, the number of milling balls has been optimized (Fig. S1, ESI†). It should be noted that the dry-milling processed Cs−Pb−Br powders were not emissive under ultraviolet (UV) light illumination. This is possibly due to the large number of defects brought by the strong mechanical shearing force, which led to severe non-radiative recombinations.[21] So, surfactants have been introduced to improve the fluorescence properties of the products (Fig. 1b). Here, 4 kinds of widely used surfactants, namely OA, OAM, BLA and OLA, have been added to the milling cans. Shown by Fourier Transform Infrared Spectroscopy (FTIR) (Fig. S2, ESI†), the signal at 1750 cm^{-1} was due to the C=O stretching vibration, and the signal that showed up near 1500 cm^{-1} belonged to the N–H blending. Thus, the successful anchoring of the surfactant on the perovskite NCs can be confirmed. Photographs of the surfactant dependent Cs−Pb−Br emitters dispersed in toluene are provided in Fig. 1c. The fluorescence properties of the synthesized powder were surfactant-dependent. According to Fig. 1c, the OAM-functionalized Cs−Pb−Br powders showed cyan emmission (R 1, G 162, B 147), while the rest exhibited blue.

The steady-state PL spectrum of the surfactant functionalized Cs−Pb−Br NCs are listed in Fig. 2a. The PL intensity peaked at 453 nm and 515 nm in the OAM-functionalized

NCs, corresponding with the cyan emission shown in Fig. 1c. Due to the lack of strong coordinative species, OA-functionalized NCs were not emissive. The PL spectrum of the OLA-functionalized Cs−Pb−Br NCs peaked at 461 nm, in agreement with the blue emission shown in Fig. 1c. Different from the photographs recorded in Fig. 1c, the BLA-functionalized NCs peaked at 513 nm, pointing to a green emission. This controversy will be discussed later coupled with the photoluminescence quantum yield (PLQY) analysis.

The transient resolved photoluminescence spectra (TRPL) curves of our synthesized NCs can be fitted with a biexponential decay mode (Fig. 2b and Table S1, ESI†). A prolonged average time constant (t_{ave}) has been observed in OAM-functionalized NCs, corresponding with a high PLQY (87.53%). This can be explained by the strong anchoring effect of the OAM surfactant. This PLQY has been reduced to 10.72% of OLA-functionalized NCs and quenched to almost zero in OA and BLA-functionalized NCs (Fig. 2c). The controversy between the photographs of UV light illumination (blue) and the steady state PL spectrum (green) was possibly due to the relatively low PLQY of the BLA-functionalized NCs.

Next came the structural characterization of the synthesized Cs−Pb−Br NCs. Here, the dispersed Cs−Pb−Br NCs solution has been mixed with polymethyl methacrylate (PMMA) and drop-coated on glass substrates for XRD characterization. The relatively strong background signals on the XRD patterns were attributed to the amorphous PMMA matrices (Fig. 2d). Interestingly, the background intensity of the OAM-functionalized emitters almost vanished, implying the high yield of the OAM-functionalized NCs. Besides, the OA showed hardly detectable signals beside the background information, this possibly suggested that OA was not effective to convert the $PbBr_2$ and CsBr reactant into the Cs−Pb−Br perovskite product during the ball-milling process. This hypothesis was further supported by the absorption spectrum (Fig. 2e). The absorption peaking at ∼310 nm for the OA-functionalized NCs basically

Fig. 2 Steady-state PL spectrum (a), TRPL curves (b) and corresponding PLQY value (c) for the OAM, OA, OLA and BLA-functionalized Cs−Pb−Br emitters. During the steady-state PL and TRPL measurements, a 400 nm laser was used for excitation. XRD patterns (d), optical absorption (e) and XPS characterization for the OAM, OA, OLA and BLA-functionalized Cs−Pb−Br emitters (f). The yellow dashed line in d could be indexed to the (002) facets of $CsPb_2Br_5$. The red dashed line points to the (100), (110), (200) and (201) facets of $CsPbBr_3$. The shaded area on the XPS characterization (f) was due to the anchoring of the organic surfactant.

rules out the existence of the Cs–Pb–Br phase. The relatively low product yield also explained the poor PLQY of the OA-functionalized NCs (Fig. 2c).

The OLA-functionalized NCs were mainly composed of $CsPb_2Br_5$, as the sharp diffraction peak at 11.6° was due to the (002) facet of $CsPb_2Br_5$ (JCPDF card # 25-0211). The XRD pattern peaked at 30.7° in the BLA-functionalized NCs, which could be indexed to the (200) facet of $CsPbBr_3$ (JCPDF card #18-0364), while $CsPbBr_3$ and $CsPb_2Br_5$ phase coexisted in the prepared OAM-functionalized NCs (Fig. 2d). As a two-dimensional (2D) inorganic perovskite halide, $CsPb_2Br_5$ exhibited an indirect band gap of 3.06 eV, larger than that of $CsPbBr_3$ (2.30 eV).[34] Listed in Fig. 2e, the absorption peak of the OLA-functionalized NCs has been blue-shifted compared with that of the OAM-functionalized samples, supporting the dominant formation of $CsPb_2Br_5$ in the OLA-functionalized NCs. As for the emission characteristics, previous studies reported the blue emission of the $CsPb_2Br_5$ NCs,[29] and a similar case was observed in our OLA-functionalized NCs. The $CsPbBr_3$ (green emitting) and $CsPb_2Br_5$ (blue emitting) mixed-phase contributed to the dual emission feature of the OAM-functionalized NCs (Fig. 2a). Special attention has been given to the signals near 400 eV in the XPS spectrum (Fig. 2f), which can be assigned to the N characteristics of the organic amine. This signal turned out to be the strongest in the OAM-functionalized Cs–Pb–Br emitters, highlighting the strong anchoring potential of the OAM surfactant.

The transmission electron microscope (TEM) characterizations have been presented in Fig. S3 (ESI†). Since the chemical exfoliation effect of OA was not effective, we especially focused on the amine-functionalized NCs. The OAM-functionalized Cs–Pb–Br emitters can be roughly divided into two kinds of nanostructures, (a) large NCs exceeding 10 nm and (b) small NCs with an average size of 5 nm. From the high-resolution TEM (HRTEM) images, a lattice spacing of 0.29 nm has been observed in the large NCs, corresponding with the (200) facet of $CsPbBr_3$ (JCPDF card #18-0364). Besides, we identified a lattice spacing of 0.76 nm in the small crystals, which could be indexed to the (002) facet of $CsPb_2Br_5$. (JCPDF card # 25-0211). The TEM characterization supported the coexistence of $CsPbBr_3$ and $CsPb_2Br_5$ in the OAM-functionalized emitters (Fig. S3e, ESI†). Distinct shuttle-shaped crystals can be observed in the OLA-functionalized NCs (Fig. S3c, ESI†), and the formation of $CsPb_2Br_5$ can be confirmed from HRTEM analysis (Fig. S3g, ESI†). The BLA-functionalized NCs were composed of $CsPbBr_3$ (Fig. S3d and h, ESI†). It should be noted that the size of the prepared OLA and BLA-functionalized NCs was much larger than that of the OAM-functionalized NCs, highlighting the excellent chemical exfoliation effect of the OAM surfactant.

The above investigations showed that the coexistence of the $CsPbBr_3$ and $CsPb_2Br_5$ phases was the reason for the dual emission. We next consider if the compositional engineering method can be used to tune the emission characteristics of the synthesized Cs–Pb–Br NCs. The following three conditions with $PbBr_2$:CsBr = 1:1; 1:1.25 and 1:1.5 were considered for further optimization. Despite the photographs of the synthesized emitters under UV illumination showing a negligible difference
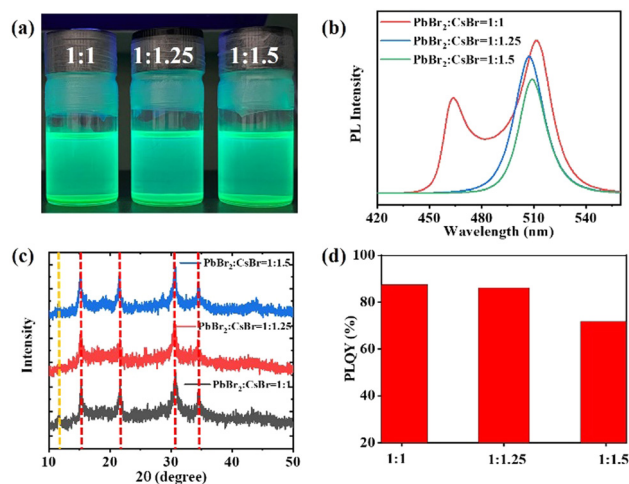

Fig. 3 (a) Photographs of the prepared Cs–Pb–Br NCs dispersed in toluene under UV light illumination. Different Cs/Pb material ratios were considered for comparison. (b) Steady-state PL spectrum, (c) XRD characterization, and (d) PLQY value of the Cs/Pb ratio dependent NCs.

(Fig. 3a), the steady-state PL spectrum suggested that the emission was largely influenced by the ratio of the precursors. Different from the Cs/Pb = 1 condition, the blue emission peak at 453 nm vanished after adding excess CsBr in the milling tank (Fig. 3b). Besides, the green emission peaked at 512 nm (Cs/Pb = 1) and has been blue-shifted with excess CsBr (Cs/Br = 1.25, Cs/Br = 1.5), pointing to a reduced defect density.[35,36] The FWHM of the synthesized Cs–Pb–Br NCs has been reduced from 25 nm (Cs/Pb = 1) to 21 nm (Cs/Pb = 1.25) and 19 nm (Cs/Pb = 1.5), verifying the high colour purity of the synthesized emitters. This reported FWHM was also among the smallest FWHM values reported by other researchers.[13,37,38]

Listed in Fig. 3c, with the increased ratio of Cs/Pb, the peak at 11.6°, which can be indexed to $CsPb_2Br_5$, disappeared. This suggested that the Cs excess processed NCs were mainly composed of $CsPbBr_3$. TEM analysis was also performed to verify this argument. Small $CsPb_2Br_5$ nanoflakes can hardly be detected in Cs/Pb = 1.25 (Fig. 4b) and Cs/Pb = 1.5 (Fig. 4c) processed NCs, confirming the phase purity of the synthesized product. It should also be noted that the PLQY reduced with the increased ratio of Cs/Pb (Fig. 3d). As for the stability concerns, the Cs–Pb–Br NCs were mixed with PMMA toluene solution and dropped coated on the glass substrates. The substrates remained highly emitting during a 2-month evaluation (Fig. S4, ESI†). Further still, we have also considered compositional
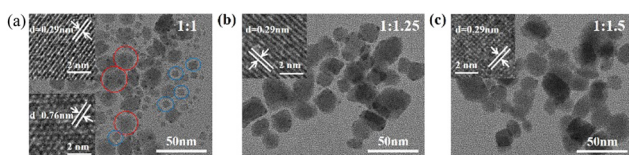

Fig. 4 TEM and the corresponding HR-TEM images of the synthesized NCs with different ratios of Cs/Pb. (a) Cs/Pb = 1 : 1, (b) Cs/Pb = 1.25, (c) Cs/Pb = 1.5. The red (blue) circled areas refer to the $CsPbBr_3$ ($CsPb_2Br_5$) phase.

varied $CsPbCl_3$ and $CsPbI_3$ emitters. Distinct blue emission can be observed from our $CsPbCl_3$ emitters, while the attempt for $CsPbI_3$ was not successful (Fig. S5 and S6, ESI†), possibly due to the transformation from the highly emitting cubic phase to the non-emitting orthorhombic polymorph.[11]

To conclude, highly emitting Cs–Pb–Br NCs have been synthesized *via* the mechanical milling method. To start with, the emitting characteristics of the synthesized NCs were largely influenced by the surfactant used in the wet-ball milling process. Compared with OA, long-chain amines such as OAM, OLA and BLA can produce emissive Cs–Pb–Br NCs. Besides, the emitting can be tuned from blue (OLA-functionalized) to cyan (OAM-functionalized) and green (BLA-functionalized) depending on the surfactant. To solve the dual emission characteristics observed in OAM-functionalized NCs, we tuned the ratio of Cs/Pb precursor added into the milling tank. Finally, with a ratio of Cs/Pb = 1.25, we received sharp (FWTH = 21 nm) green-emitting Cs–Pb–Br NCs with relatively high PLQY (86.11%). The current research demonstrated the effectiveness of mechanical milling to synthesize highly emitting compositional and structural tuning Cs–Pb–Br emitters.

Conflicts of interest

There are no conflicts to declare.

Notes and references

1 Y. Bai, Z. Huang, X. Zhang, J. Z. Lu, X. X. Niu, Z. W. He, C. Zhu, M. Q. Xiao, Q. Z. Song, X. Y. Wei, C. Y. Wang, Z. H. Cui, J. Dou, Y. H. Chen, F. T. Pei, H. C. Zai, W. Wang, T. L. Song, P. F. An, J. Zhang, J. C. Dong, Y. M. Li, J. J. Shi, H. B. Jin, P. W. Chen, Y. C. Sun, Y. J. Li, H. N. Chen, Z. M. Wei, H. P. Zhou and Q. Chen, *Science*, 2022, **378**(6621), 747–754.
2 L. Liu, A. Najar, K. Wang, M. Y. Du and S. Z. Liu, *Adv. Sci.*, 2022, **9**(7), 2104577.
3 J. Yang, Q. Bao, L. Shen and L. Ding, *Nano Energy*, 2020, **76**, 105019.
4 K. Lin, J. Xing, L. N. Quan, F. P. G. de Arquer, X. W. Gong, J. X. Lu, L. Q. Xie, W. J. Zhao, D. Zhang, C. Z. Yan, W. Q. Li, X. Y. Liu, Y. Lu, J. Kirman, E. H. Sargent, Q. H. Xiong and Z. H. Wei, *Nature*, 2018, **562**(7726), 245–248.
5 X. B. Tang, N. L. Kothalawala, Y. L. Zhang, D. L. Qian, D. Y. Kim and F. Q. Yang, *Chem. Eng. J.*, 2021, **425**, 131456.
6 H. Huang, C. Zuo, H. Zeng and L. Ding, *J. Semicond.*, 2021, **42**(3), 030202.
7 L. Zhang, X. Pan, L. Liu and L. Ding, *J. Semicond.*, 2022, **42**(3), 030203.
8 L. T. Dou, Y. Yang, J. B. You, Z. R. Hong, W. H. Chang, G. Li and Y. Yang, *Nat. Commun.*, 2014, **5**(1), 5404.
9 J. G. Feng, X. X. Yan, Y. Liu, H. F. Gao, Y. C. Wu, B. Su and L. Jiang, *Adv. Mater.*, 2017, **29**(16), 1605993.
10 F. Yan and H. V. Demir, *Nanoscale*, 2019, **11**(24), 11402–11412.
11 Q. X. Zhong, M. H. Cao, Y. F. Xu, P. L. Li, Y. Zhang, H. C. Hu, D. Yang, Y. Xu, L. Wang, Y. Y. Li, X. H. Zhang and Q. Zhang, *Nano Lett.*, 2019, **19**(6), 4151–4157.
12 Q. G. Zhang, W. L. Zheng, Q. Wan, M. M. Liu, X. P. Feng, L. Kong and L. Li, *Adv. Opt. Mater.*, 2021, **9**(11), 2002130.
13 E. Erol, O. Kibrisli, M. C. Ersundu and A. E. Ersundu, *Chem. Eng. J.*, 2020, **401**, 126053.
14 L. Protesescu, S. Yakunin, M. I. Bodnarchuk, F. Krieg, R. Caputo, C. H. Hendon, R. X. Yang, A. Walsh and M. V. Kovalenko, *Nano Lett.*, 2015, **15**(6), 3692–3696.
15 D. D. Yan, Q. H. Mo, S. Y. Zhao, W. S. Cai and Z. G. Zang, *Nanoscale*, 2021, **13**(21), 9740–9746.
16 J. F. Liao, Y. F. Xu, X. D. Wang, H. Y. Chen and D. B. Kuang, *ACS Appl. Mater. Interfaces*, 2018, **10**(49), 42301–42309.
17 S. X. Wang, C. H. Bi, J. F. Yuan, L. X. Zhang and J. Tian, *ACS Energy Lett.*, 2018, **3**(1), 245–251.
18 J. F. Cao, Z. D. Yin, Q. Pang, Y. X. Lu, X. Q. Nong and J. Z. Zhang, *J. Chem. Phys.*, 2021, **155**(23), 234701.
19 Y. T. Cai, P. J. Zhang, W. H. Bai, L. Lu, L. Wang, X. Chen and R. J. Xie, *ACS Sustainable Chem. Eng.*, 2022, **10**(22), 7385–7393.
20 J. K. Park, J. H. Heo, B. W. Kim and S. H. Im, *J. Ind. Eng. Chem.*, 2020, **92**(25), 167–173.
21 L. Wang, D. C. Ma, C. Guo, X. Jiang, M. L. Li, T. T. Xu, J. P. Zhu, B. B. Fan, W. Liu, G. Shao, H. L. Xu, H. L. Wang, R. Zhang and H. X. Lu, *Appl. Surf. Sci.*, 2021, **543**(30), 148782.
22 Z. Y. Zhu, Q. Q. Yang, L. F. Gao, L. Zhang, A. Y. Shi, C. L. Sun, Q. Wang and H. L. Zhang, *J. Phys. Chem. Lett.*, 2017, **8**(7), 1610–1614.
23 S. Kumar, M. Regue, M. A. Isaacs, E. Freeman and S. Eslava, *ACS Appl. Energy Mater.*, 2020, **3**(5), 4509–4522.
24 L. Protesescu, S. Yakunin, O. Nazarenko, D. N. Dirin and M. V. Kovalenko, *ACS Appl. Nano Mater.*, 2018, **1**(3), 1300–1308.
25 Y. Li, H. Huang, Y. Xiong, S. V. Kershaw and A. L. Rogach, *CrystEngComm*, 2018, **20**(34), 4900–4904.
26 G. Maity and S. K. Pradhan, *J. Alloys Compd.*, 2020, **816**(5), 152612.
27 S. K. Balakrishnan and P. V. Kamat, *Chem. Mater.*, 2018, **30**(1), 74–78.
28 A. F. V. da Fonseca, B. R. C. Vale, T. A. D. S. Carvalho, J. Bettini, A. C. Pereira and M. A. Schiavon, *J. Phys. Chem. C*, 2021, **125**(49), 27363–27371.
29 C. Collantes, V. G. Pedro, M. J. Bañuls and Á. Maquieira, *ACS Appl. Nano Mater.*, 2021, **4**(2), 2011–2018.
30 Q. Jing, Y. Xu, Y. C. Su, X. Xing and Z. D. Lu, *Nanoscale*, 2019, **11**(4), 1784–1789.
31 B. S. Zhu, H. Z. Li, J. Ge, H. D. Li, Y. C. Yin, K. H. Wang, C. Chen, J. S. Yao, Q. Zhang and H. B. Yao, *Nanoscale*, 2018, **10**(41), 19262–19271.
32 G. C. Jiang, C. Guhrenz, A. Kirch, L. Sonntag, C. Bauer, X. L. Fan, J. Wang, S. Reineke, N. Gaponik and A. Eychmüller, *ACS Nano*, 2019, **13**(9), 10386–10396.
33 K. Y. Baek, W. Lee, J. Lee, J. Kim, H. Ahn, J. I. Kim, J. Kim, H. Lim, J. Shin, Y. J. Ko, H. D. Lee, R. H. Friend, T. W. Lee, J. Lee, K. Kang and T. Lee, *Nat. Commun.*, 2022, **13**(1), 4263.
34 P. Acharyya, P. Pal, P. K. Samanta, A. Sarkar, S. K. Pati and K. Biswas, *Nanoscale*, 2019, **11**(9), 4001–4007.
35 S. Yang, J. Dai, Z. H. Yu, Y. C. Shao, Y. Zhou, X. Xiao, X. C. Zeng and J. S. Huang, *J. Am. Chem. Soc.*, 2019, **141**(14), 5781–5787.
36 B. H. Zhao, X. Y. Yan, T. Zhang, X. T. Ma, C. B. Liu, H. Y. Liu, K. Y. Yan, Y. L. Chen and X. Y. Li, *ACS Appl. Mater. Interfaces*, 2020, **12**(8), 9300–9306.
37 Z. C. Li, L. Kong, S. Q. Huang and L. Li, *Angew. Chem., Int. Ed.*, 2017, **56**(28), 8134–8138.
38 Z. T. Wang, R. Fu, F. Li, H. D. Xie, P. W. He, Q. Sha, Z. B. Tang, N. Wang and H. Z. Zhong, *Adv. Funct. Mater.*, 2021, **31**(22), 2010009.